TPM Vol. 32, No. S3, 2025
ISSN: 1972-6325
https://www.tpmap.org/

Open Access

EXPERIMENTAL STUDY IN A WIND TUNNEL AND IN CFD OF THE DISTRIBUTIONS OF SPEEDS AND PRESSURES ON A DOMED HOUSE

[1]NOEMI GERALDINE PEREZ LAURA, [2]KEVIN ROMARIO CHUCKON SUNCION, [3]BEL CARMONA ARTEAGA, [4]JHON HENRY RODRIGUEZ POMAJULCA
[1,2,3,4]UNIVERSIDAD PRIVADA DEL NORTE

ABSTRACT: Dome-shaped constructions were used from the period of the great civilizations and until today, around the world we have great architectural examples of the use of this form, also in Peru we can also find a relevant case which are the trulys, eco-friendly homes. friendly and dome-like. In the context of studying these structures, they addressed the shape, stability and resistance, but in the context of aerodynamics and housing, very few studies have been carried out. Therefore, our research is based on designing a dome-shaped housing model based on a mathematical equation in order to analyze its aerodynamic behavior experimentally and computationally from the distributions of speeds and pressures. Technological advances allowed us to carry out this study with the help of computer software. Carrying out the simulation in Autodesk CFD and in the same way the solid in physics at scale in the wind tunnel using air as a fluid, which was subjected to different speeds and pressures in order to analyze if the solid complies with the aerodynamics both experimentally and computationally it is expected to be a reference for larger scale research**.**

Keywords:*CFD, speeds, pressures, cupola, aerodynamic*

1. INTRODUCTION

Dome-shaped constructions have been the object of study during the period of the great civilizations, which were used for the construction of temples, palaces and public buildings. To this day, such infrastructures remain as referents of engineering and architecture due to their structural characteristics and advantages [1].
In history, a preeminent advantage according to the French scientist Pierre Bouguer (1734), is that "concave and conical shapes are always stable thanks to the ability of domes to develop annular compressive stresses" [2]. The above-mentioned by the author refers to the fact that the weight of the structure is evenly distributed along its curved shape, which allows it to be more seismic-resistant and stable.
The use of the dome begins in the Mycenaean civilization [3], however, around the world we have great architectural references such as: The dome of Hagia Sophia, Turkey (532 - 537 CE), the dome of Santa Maria di Fiore, Italy (15th century), the dome of St. Paul's, London (17th century) and the dome of St. Peter's, Rome (18th century), these are some examples around the world [2] [4].
In Peru, we also have architectural references, a relevant example of which is found in the town of Pasamayo, called Trulys, which is an eco-friendly structure because it is built of mud and quincha with a dome-shaped design [5], this can be seen in Figure 1.
The interaction between wind and architectural structures has been studied for decades [6]. In the case of aerodynamic dwellings, this relationship is viewed from a different perspective. Unlike buildings or skyscrapers, dwellings do not usually face critical aerodynamic forces, which may not warrant detailed wind impact studies. In addition, aerodynamic studies can be costly and complex, which discourages them in housing projects, where budgets and design prioritize other features.

Fig. 1 Housing trulys. [7].

In order to carry out the study of the present research, it is of great importance to understand in detail how air currents affect these surfaces, thanks to technological progress this is possible, performing computational fluid dynamics (CFD) simulations and wind tunnel experiments in a practical and low-cost way.
For the aforementioned reasons, a housing model was designed based on a dome-shaped mathematical equation in order to analyze the velocity and pressure distributions by means of aerodynamic study.

2. THEORETICAL FRAMEWORK

2.1 CalPlot 3

It is an interactive three-dimensional surface plotter that allows you to plot functions, curves in space, implicit surfaces, vector fields and solids of revolution **[8]**.

2.2 Autodesk Fusion

It is a cloud-based 3D modeling, CAD, CAM, CAE and PCB software for quality product design and manufacturing **[9]**.

2.3 Autodesk Inventor Professional

It is a 3D CAD software that offers 3D mechanical design tools, documentation issuance and product simulation in professional quality **[10]**.

2.4 Autodesk CFD

Autodesk CFD (Computational Fluid Dynamics) is a software that creates digital simulations understanding fluid dynamics, in which engineers and analysts use to know precisely the behavior of gases, liquids and air **[11]**.

2.5 Reynolds numbers

It is one of several dimensionless numbers that are useful in the study of fluid mechanics and heat transfer, it is used to determine what type of motion a fluid has, whether laminar, transitional or turbulent **[12]**. Equations 1 and 2 show the hydraulic diameter and Reynolds number.
If Re < 2300, the flow is laminar.
If Re ≥ 2300, the flow is turbulent.

$$D_h = \frac{4ab}{2a+b}. \quad (1)$$

$$R_e = \frac{\rho V D_h}{\mu} \quad (2)$$

The variables in question are as follows:
Re = Reynolds number.
$\boldsymbol{\rho}$ = Fluid density (kg/m3).
V = Fluid velocity (m/s).
Dh = Hydraulic diameter (m).
μ = Dynamic viscosity of the fluid (N.s/m2).

2.6 Energy equation

The energy equation is an extension of Bernoulli's equation, which aims to solve situations of energy losses and gains by analyzing the behavior of a fluid **[13]**. The energy formula is shown in equation 3.

$$\frac{v_1^2}{2g} + \frac{P_1}{\gamma} + Z_1 = \frac{v_2^2}{2g} + \frac{P_2}{\gamma} + Z_2 + ht \quad (3)$$

The variables in question are as follows:
$\boldsymbol{v_1}$ = Input velocity load.
$\boldsymbol{v_2}$ = Outlet velocity load.
$\boldsymbol{\gamma}$ = Specific gravity of the fluid.
$\boldsymbol{P_1}$ = Inlet pressure load.
$\boldsymbol{P_2}$ = Outlet pressure load.
$\boldsymbol{Z_1}$ = Height of the first section.
$\boldsymbol{Z_2}$ = Height of the second section.
g = Gravity.
$\boldsymbol{h_T}$ = Total losses.

2.7 Dragging force.

TPM Vol. 32, No. S3, 2025
ISSN: 1972-6325
https://www.tpmap.org/

Open Access

Drag force is the resistance force experienced by a solid subjected to the thrust of a fluid. This force depends on the properties of the fluid and the solid **[14]**. Equation 4 visualizes the drag force.

$$F_D = C_D \times A \times \frac{V^2 \times \rho}{2} \qquad (4)$$

The variables in question are as follows:
FD = Draf force.
CD = Drag coefficient.
A = Frontal area.
V = Fluid velocity.
ρ = Fluid density.

2.8 Von Karman Effect

The Von Karman effect refers to swirling, confined flows with very high Reynolds numbers in relatively small volumes. As the flow approaches the front surface of the detaching element, it splits into two streams. The fluid near the body moves at a lower velocity compared to the main flow velocity. This difference in velocities results in the formation of shear layers, which eventually break into alternating vortices on both sides of the detachment element **[15]**.

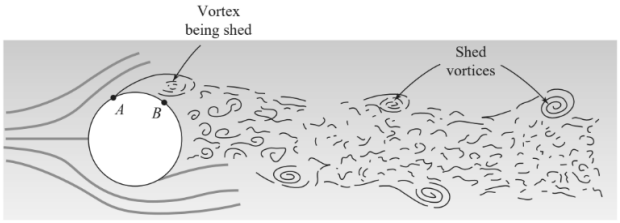

Fig. 3 Drawing of vortices detaching from a circular element. **[15]** .

2.9 Release point

The release point or also called detachment point is the result of the dispersion of the fluid velocity generating vortices in the wake, known as vortex detachment **[16]**.

2.10 Stagnation point

The stagnation point is described as the point where the velocity is zero, this is within the flow field. Fig. 4 details precisely the stagnation point, detachment point and wake generated by the element **[17]**.

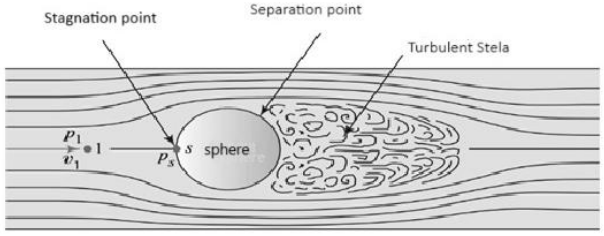

Fig. 4 Fluid behavior with a spherical profile showing the stagnation point and the turbulent wake **[17]**.

3. METHODOLOGY

In the present investigation the methodology was detailed by means of two flowcharts, Figure 5 shows the detail of the design and experimental study while Figure 6 shows the computational study in CFD. For further analysis of the solid, Figure 7 shows the fusion meshing.

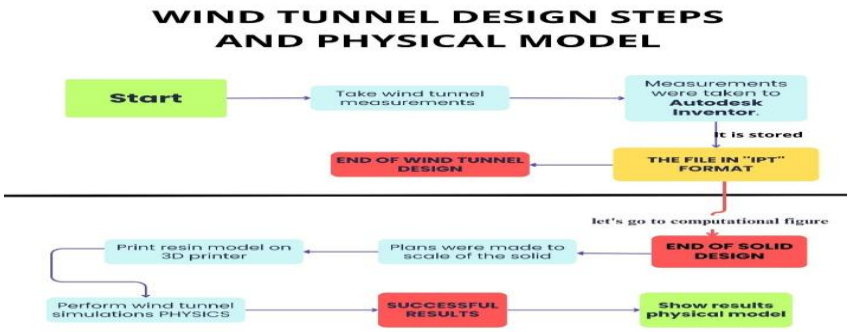

Fig. 5 Steps for the design and wind tunnel simulation of the physical model.(Own elaboration)

TPM Vol. 32, No. S3, 2025
ISSN: 1972-6325
https://www.tpmap.org/

Open Access

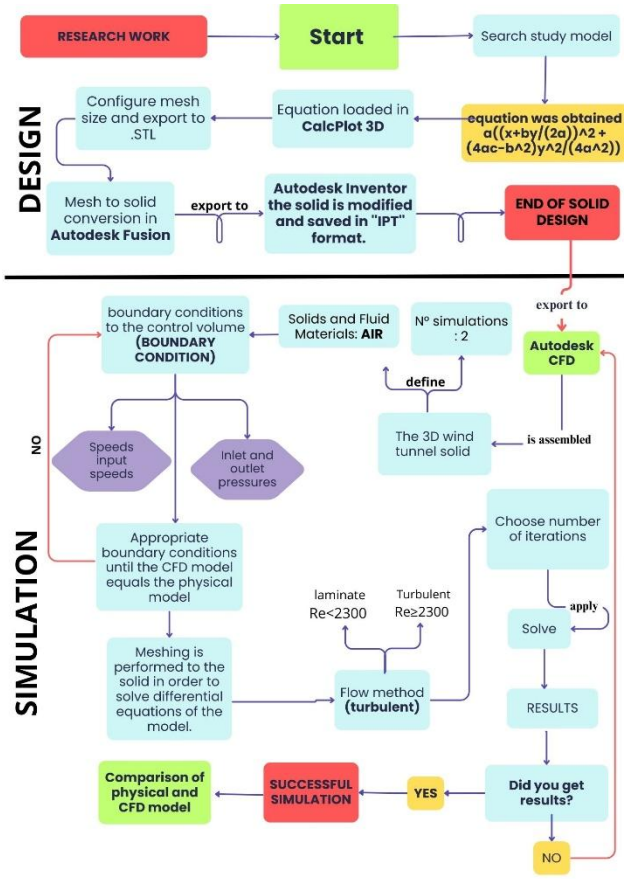

Fig. 6 Steps for the design and simulation of the wind tunnel and CFD model. (Own elaboration)

4. RESULTS

The analysis of the behavior of the velocities and pressures of the dome-shaped model was carried out using Autodesk CFD software.

Before carrying out the simulation, certain air flow conditions were taken into account, which were that the flow was incompressible, ideal, permanent and confined. Also, that the density was constant, which we know is not true in real life, but given the complexity of the study, these variations were assumed.

Velocity values of 1.06 m/s and 2.10 m/s were used for the wind tunnel input of the CFD simulation. In turn, the gauge pressures at the system inlet was 30 Pa and 0 Pa at the outlet. The simulations were performed taking into account that the fluid condition was turbulent using an SST K-Omega SAS model. In this way, the study of the aerodynamics of the model was analyzed for its velocity and pressure distributions.

4.1 Velocity distribution analysis with 1.06 m/s

After carrying out the simulation with 2000 iterations, a solution was obtained in iteration number 231. In Figure 7, profile view, it was observed that the inlet velocities range between 0.84 m/s and 1.26 m/s. As the flow advanced, we visualized how the colorimetry varied, indicating the increase in velocity as the wind tunnel area is reduced until reaching the central zone between the model and the sensor, reaching a range of maximum velocities between 7.54 m/s and 8.38 m/s.

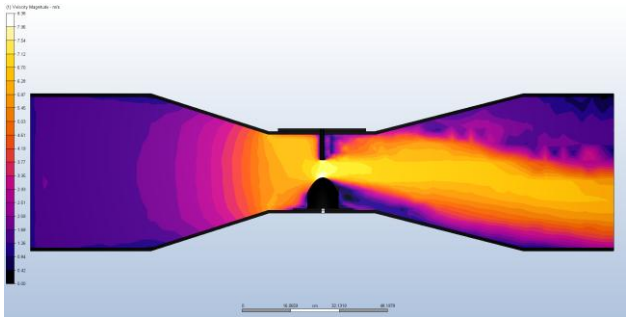

Fig.7 Velocity distribution for inlet conditions of 1.06 m/s in profile view.

In Figure 8, plan view, the stagnation point was observed at the moment when the flow made contact with the model in the upper part of the model, oscillating between velocities of 0.00 m/s and 2.09 m/s. In addition, the separation points formed on the sides presented regular velocities between 4.61 m/s and 5.45 m/s until the turbulent wake was generated with velocities between 0.00 m/s and 2.93 m/s.

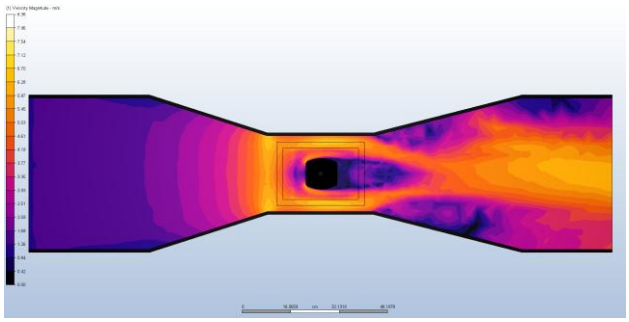

Fig.8 Velocity distribution for inlet conditions of 1.06 m/s in plan view.

In Figure 9, front view, it was noticeably observed that high velocities were obtained around the model. Thus, in the upper part of the simulation, the maximum velocity, specifically 8.38 m/s, was reached.

Fig.9 Velocity distribution for inlet conditions of 1.06 m/s in front view.

In Figure 10, it was possible to visualize the velocity direction of the vectors, where it was observed that the wind direction in the right section of the dome-shaped model rotated in the opposite direction, called vorticity, demonstrating that this surface is aerodynamic and an efficient dissipator. The initial velocity increases progressively due to the reduction of the areas in the wind tunnel and, upon impact with the model, turbulence is generated where the velocities became zero.

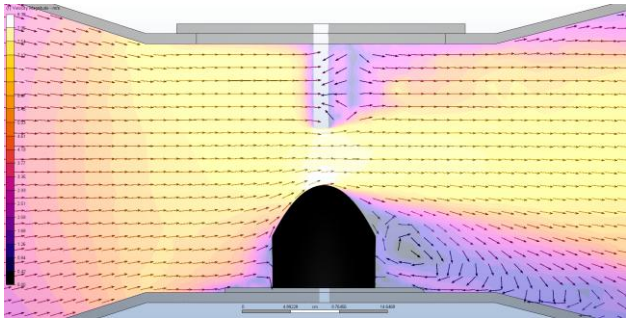

Fig10. Velocity vector distribution for input conditions of 1.06 m/s in profile view.

4.2 Velocity distribution analysis with 2.10 m/s.

A solution was obtained in iteration number 502. In Figures 11, 12 and 13, in front, plan and profile views respectively, it was seen that, in the central area of the simulation, which is shared between our model and the sensor, there was an increase in velocity ranging from 8.07 m/s to 10.09 m/s. This indicated that the flow velocity increases in this area due to the reduction in cross section. We then observed that the flow, as it passed through the model and the sensor, began to change velocity, as demonstrated by the color scale. Thus, the flow distribution took on an acceleration and deceleration pattern in different areas.

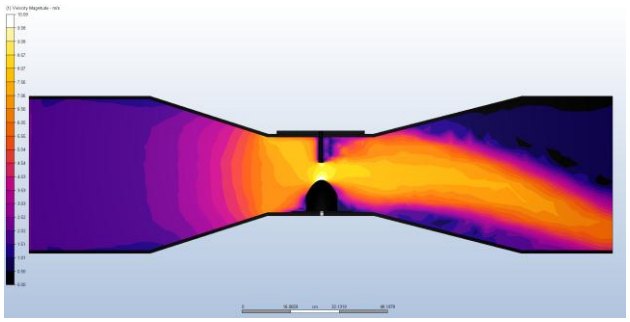

Fig.11 Velocity distribution for inlet conditions of 2.10 m/s in profile view.

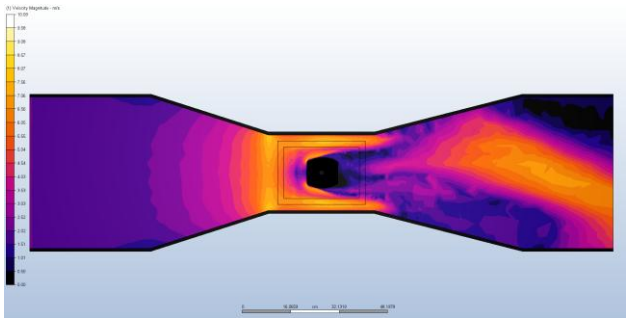

Fig.12 Velocity distribution for inlet conditions of 2.10 m/s in plan view.

Fig.13 Velocity distribution for input conditions of 2.10 m/s in front view.

In Figure 14, we visualize the shape of our model, as flow return zones are created. The velocity vectors around the model show abrupt changes in both direction and magnitude, generating turbulence and vorticity.

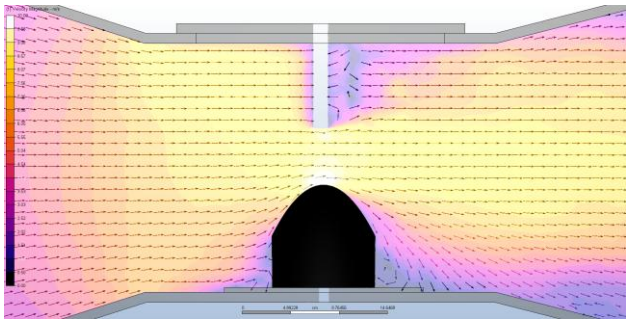

Fig.14 Velocity vector distribution for 2.10 m/s input conditions in profile view.

4.3 Analysis of pressure distributions with 30 Pa for 1.06 m/s.

In Figures 15, in profile view, the pressure distributions throughout the simulation were presented visually by means of a colorimetric range, where the inlet pressure decreased as it traveled through the model. In the middle zone it reached a pressure of 10.60 Pa. Also, we observed that the pressure when contacting the sensor and the model reached again its maximum pressure due to the stagnation of the flow. In addition, negative pressures ranging from 34.68 Pa to 12.04 Pa were generated at the top of the model and the sensor, due to the principle of the energy equation.

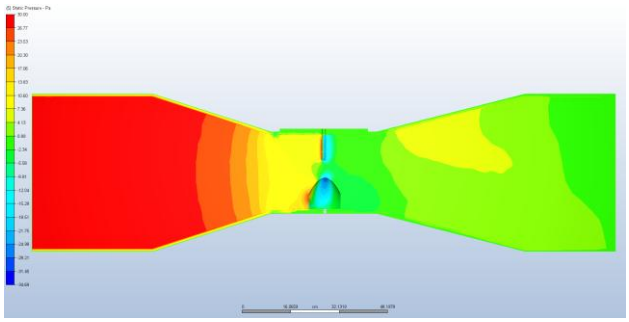

Fig.15 Pressure distribution for inlet conditions of 30 Pa for 1.06 m/s in profile view**.**

In Figure 16, in plan view, it was observed that, in the central area of the simulated tunnel, the pressure in contact with the model increases, oscillating between 10.60 Pa and 20.30 Pa. At the same time, as the flow moves away from the model, the pressure in certain areas increases and decreases due to the effect of velocity.

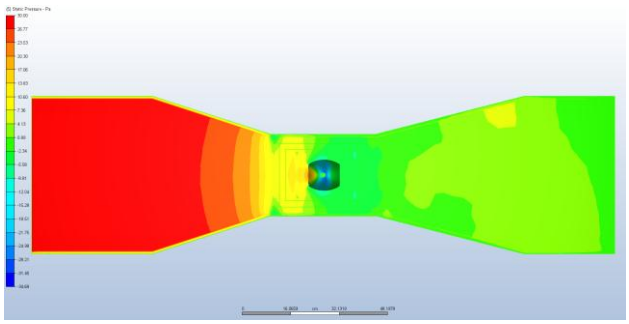

Fig16. Pressure distribution for inlet conditions of 30 Pa for 1.06 m/s in plan view.
In Figure 17, front view, shows that the pressures on the surface of the model are relatively low, being light blue and shades of green, with an estimated range between -18.51 Pa and -2.34 Pa.

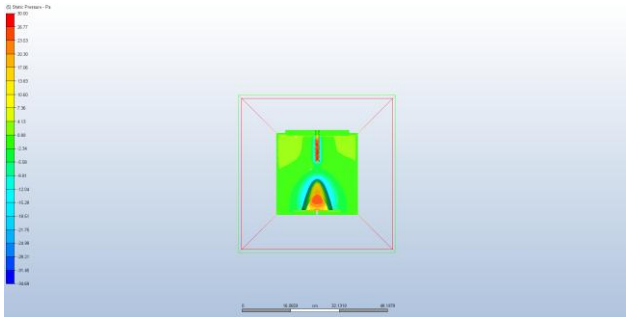

Fig.17 Pressure distribution for inlet conditions of 30 Pa for 1.06 m/s in front view.

4.4 Analysis of pressure distributions with 30 Pa for 2.10 m/s.

The representations of the profile, plan and frontal views, respectively, are shown in Figures 18, 19, 20. In these graphical representations, we identify that the stagnation point zone presents pressures between 24.06 Pa and 32.95 Pa. In turn, in the upper zone of the cupular model we can visualize the lowest pressure point, which is -55.93 Pa. In Figures 18 19 20, the flow, after passing through the sensor and the model, progressively changes the color scale, increasing the pressure. In Figure 20, the sides of the model surface present negative charges between 33.71 Pa and 24.82 Pa, which are identified with light blue shades.

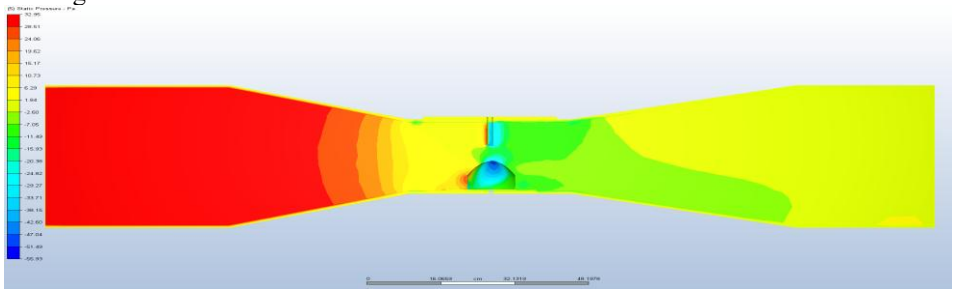

Fig.18 Pressure distribution for inlet conditions of 30 Pa for 2.10 m/s in profile view.

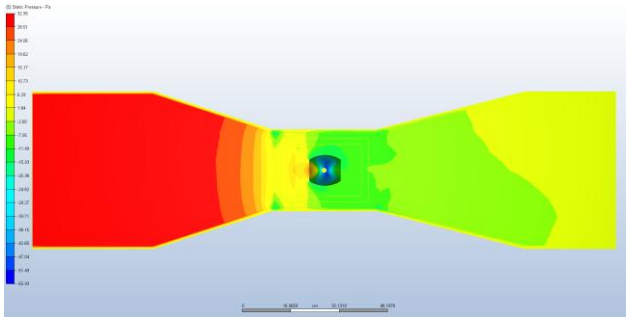

Fig.19 Pressure distribution for inlet conditions of 30 Pa for 2.10 m/s in plan view.

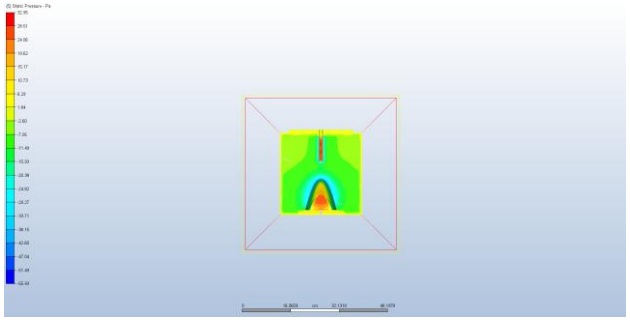

Fig.20 Pressure distribution for inlet conditions of 30 Pa for 2.10 m/s in front view.

4.5 Simulations using the wind tunnel.

Experimentally, in the laboratory wind tunnel, it was possible to visualize the interaction of the wind with the printed solid, in which the forces of dragging, detachment and stagnation converge, as shown in Figures 21 and 22.

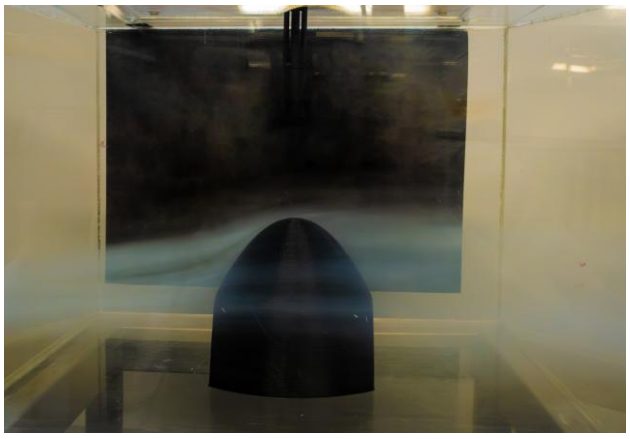

Fig.21 Wind tunnel simulation of the velocity at the 4.27m/s sensor.

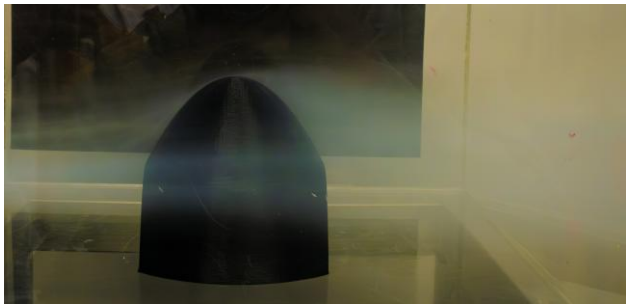

Fig.22 Wind tunnel simulation of the velocity at 8.40m/s sensor.

5. CONCLUSION

In this research, it was possible to demonstrate that the analysis performed with the Autodesk CFD simulator, the dome-shaped model has aerodynamic characteristics that allow an efficient management of the air flow. The tests performed in the simulator show an increase in flow velocity in areas of reduced area that, upon impact with the model, generate stagnation points and turbulence on the surface. Likewise, low pressure zones are created, even reaching negative values, due to the principle of the energy equation. This behavior is fundamental to understand the stability and structural resistance of the model under different wind conditions.

REFERENCES

[1] G. Lopez, "Technical reports and theoretical studies about the structural behaviour of masonry domes in the 18th century," Frontiers of Architectural Research, vol. 12, iss. 1, pp. 42-
[2] G. Lopez, "La forma ideal de las cúpulas: el ensayo de Bouguer," Actas del III Congreso Nacional de Historia de la Construcción, Sevilla 26–28 octubre de 2000, Madrid: Instituto Juan de Herrera, 2000, pp. 603-613. https://www.sedhc.es/biblioteca/actas/CNHC3_070.pdf
[3] S. Arboleya, "Constructive-structural analysis: dome of the church of the Universidad Laboral de Gijón," Dept, Higher Technical School of Architecture, Of A Coruña Univ., A Coruña, 2020. https://ruc.udc.es/dspace/handle/2183/26269
[4] L. Prado, "Análisis estructural de la cúpula de Santa Sofía," Dept, Estructuras y Física de Edificación., Politécnica de Madrid Univ., Madrid, 2022. https://oa.upm.es/69681/
[5] Z. Bendezú, A. Clementina, "Análisis del turismo vivencial en la finca ecológica Ecotruly Park, 2019," Dept. Ciencias Empresariales., Cesar Vallejo Univ., Lima, 2019. https://repositorio.ucv.edu.pe/handle/20.500.12692/54497
[6] M. C. Modesto Monedero, "Evolución de los edificios en altura después del periódo icónico: análisis del desarrollo formal en la edificación en altura mediante la simulación fluidodinámica de la acción del viento (CFD)," Projecte Final de Màster Oficial, UPC, Escola Tècnica Superior d'Arquitectura de Barcelona, Departament d'Enginyeria de la Construcció, 2009.
[7] J. Arévalo, "Eco Truly Park: cómo llegar y cuánto cuesta hospedarse en este refugio espiritual y recinto de yoga," El Comercio, Jun 31, 2023. [Online]. Available: El Comercio, https://elcomercio.pe/vamos/peru/eco-truly-park-como-llegar-cuanto-cuesta-y-que-tiene-de-diferente-este-lugar-turistico-lima-huaral-noticia/ [Accessed, Jun 31, 2023].
[8] P. Seeburger, "CalcPlot 3D (version en español)," Merlot, Jun 13, 2023. [Online]. Available: Merlot, https://www.merlot.org/merlot/viewMaterial.htm?id=773415523 [Accessed, Jun 13, 2023].
[9] Autodesk Inc, "Autodesk Fusion: More than CAD, it´s the future of design and manufacturing," Autodesk, [Online]. Available: Autodesk Inc, https://dotcom-aem.efddotcom.autodesk.com/products/fusion-360/overview?term=1-YEAR&tab=subscription [Accessed, 2024].
[10] Autodesk Inc, "Autodesk Inventor: 3D modelling software for designers and engineers," Autodesk, [Online]. Available: Autodesk Inc, https://www.autodesk.com/products/inventor/overview?us_oa=dotcom-us&us_si=739505c5-6f49-41bd-be6c-c96d127459fa&us_st=inventor&us_pt=INVNTOR [Accessed, 2024].
[11] Autodesk Inc, "Autodesk CFD: Simulation software for engineering complex liquid, gas, and air systems," Autodesk, [Online]. Available: Autodesk Inc, https://www.autodesk.com/products/cfd/overview?term=1YEAR&tab=subscription [Accessed, 2024].
[12] Y. A. Cengel and J. M. Cimbala, Mecánica de Fluidos Fundamentos y Aplicaciones, 1st ed. Mc Graw Hill, 2015.
[13] L. Peiging, Z. Yunke, "THE HISTORICAL CONTRIBUTION OF BERNOULLI'S EQUATION TO THE ESTABLISHMENT OF FLUID MECHANICS THEORY," MECHANICS IN ENGINEERING, vol. 42, no. 2, pp. 258-264, Abril. 2020, https://dx.doi.org/10.6052/1000-0879-19-179
[14] R.L. Mott and J.A. Untener, Mecánica de Fluidos, 7ma ed. Addison Wesley, 2015, pp. 181-182.
[15] M. Sánchez, R. Atienza, and D. Yañez, "DISEÑO Y OPTIMIZACION DE UNA ESTRUCTURA GEOMÉTRICA CILINDICA PARA UN DESPRENDIMIENTO UNIFORME DE VORTICES DE VON KARMAN," Tecnología y Desarrollo, vol. 15, iss. 1696-8085, May. 2017. https://revistas.uax.es/index.php/tec_des/article/view/1181/969
[16] L.D. Landau, E.M. Lifshitz, L.P. Pitaevskii, and V.B. Berestetskii, Mecánica de Fluidos volumen 6, Ed. Madrid: Reverté, 2021, p.24.
[17] E. Morente, "Estudio del efecto del borde de salida en el desprendimiento de vórtices generado por una cascada de álabes," Politécnica de Catalunya Univ., Cataluña, 2019.